Ocean Modelling 103 (2016) 38–52

Contents lists available at ScienceDirect

Ocean Modelling

journal homepage: www.elsevier.com/locate/ocemod

Virtual Special Issue
Ocean Surface Waves

Characteristics of directional wave spectra and implications for detailed-balance wave modeling

Donald T. Resio[a,*], Linwood Vincent[b], Dorukhan Ardag[a]

[a] College of Computing, Engineering and Construction, University of North Florida, Jacksonville, FL 32224, United States
[b] University of Miami, Miami, FL, United States

ARTICLE INFO

Article history:
Received 23 February 2015
Revised 28 September 2015
Accepted 30 September 2015
Available online 8 October 2015

Keywords:
Directional wave spectra
Wave modeling

ABSTRACT

There is an increasing need for accurate wave spectra in remote sensing applications and for accurate estimates of momentum exchanges between waves and the atmosphere and ocean in coupled modeling. Existing operational models are calibrated in a holistic context which focuses on integrated wave growth and dissipation, not on the detailed-balance exchanges required for these emerging needs. Here we propose a set of metrics, based on a number of careful observational studies, for use in future model evaluations. An overall perspective seen in the observational data is a general agreement with shapes anticipated from energy, action and momentum flux constraints produced by nonlinear wave interactions in wave spectra. Given the apparent importance of the nonlinear source term to detailed-balance model, we review the basis of the existing approximation used in existing operational models and find this form deviates significantly from the full integral representation of these interactions. It is proposed here that new observational evidence and theoretical formulations be utilized in the development of wave models specifically to meet remote sensing and coupled modeling needs.

1. Introduction

The accuracy of operational wind-wave models has continued to increase in recent years (Alves et al., 2002; Ardhuin et al., 2007, 2010; Chao et al., 2005; Siadatmousavi et al., 2012; Tolman, 2004; Tolman and Grumbine, 2013), at least in terms of the ability to predict integrated wave parameters, such as wave heights based on total energy, mean wave period and mean propagation direction. Much of this progress was accomplished via empirical model tuning to fit observations; and, as pointed out in WAMDIG (1988), although such optimization can produce high-quality results in many areas of the world, it does not ensure that such models accurately represent the detailed balance of energy, action and momentum within wave spectra. This leads to modeled spectral shapes that can deviate markedly from observed spectral shapes, even in situations where modeled and measured integrated parameters are highly correlated, as shown by Figs. 7–9 in Montoya et al. (2013).

An important component in ongoing global environmental research is the increasing effort directed toward building coupled models of the earth's marine weather and climate. In such modeling systems, waves often act as an intermediary between ocean and atmosphere processes; and it is critical that wave models accurately represent fluxes of momentum and energy between the atmosphere and wind waves and between wind waves and the ocean. The frequency–direction location at which energy enters and leaves a wave spectrum is necessary for accurately predicting spectral shape evolution as well as for quantifying the role of waves in coupled models, since the momentum flux associated with such exchanges depends on both the phase speed and propagation direction of the waves involved. For example, off the Northwest Coast of North America, strong winds and high wave conditions are dominant, especially in winter, with winds often reaching 30 m/s, and significant wave heights in excess of 8 m. In these conditions, impacts on ocean mixing are large, owing to wave breaking and Langmuir turbulence, dramatically increasing upper ocean turbulent kinetic energy and affecting Ekman surface currents, and other currents (D'Asaro, 2014: D'Asaro et al., 2014).

An example of the importance of a detailed balance characterization of wave model source terms can be found in existing interpretations for wave breaking, S_{ds}, typically observed to occur physically on the leading face of waves or near the wave crest. Two different physical interpretations of this phenomenon have been

* Corresponding author. Tel.: +1 904 620 2695.
E-mail address: Don.Resio@unf.edu (D.T. Resio).

http://dx.doi.org/10.1016/j.ocemod.2015.09.009
1463-5003/

postulated. Alves and Banner (2003) argue that the most dissipation occurs in the spectral peak region of the spectrum due to energy convergence at frequencies near the spectral peak in young seas. On the other hand, Irisov and Voronovich (2010) theorize that such breaking is related to stretching and convergence of shorter waves by the longer waves, within the theoretical framework developed by Longuet-Higgins and Cokelet (1976, 1978) as discussed in Longuet-Higgins (1988). For the same amount of energy loss from a wave field, the momentum transferred into the ocean under the latter interpretation could be two to three times higher than that based on the assumption of primary dissipation at frequencies near the spectral peak. Thus, a reasonable prediction of a net energy balance does not ensure that momentum transfer rates will be predicted equally well. The need for accurate detailed-balance source terms is also critical to many remote sensing applications since such information is often inferred from a given portion of the spectrum. For example, high-resolution marine wind estimates can be retrieved from satellite imagery, based on backscatter from capillary waves (Zhang and Perrie, 2012; Zhang et al., 2012). Since capillary waves are likely to be very coupled to fluxes entering from very-high frequency gravity waves and capillary-gravity waves, improvements in representations of spectral shape in the high-frequency gravity-wave portion of the spectrum could spawn a better understanding of the physics responsible for producing the overall energy levels within the capillary range.

We see from the previous discussion that there is a strong motivation to develop objective metrics for use in evaluating detailed balance-formulations within wave models. In this paper, primary interest will be focused on the nonlinear interaction source term, S_{nl}, since it is the one term which is known from first principles and has long been recognized as a primary mechanism for redistributing energy within the spectrum. Also, this source term is considered by many as a critical shape stabilizing mechanism (Hasselmann et al., 1976; Kitaigorodskii, 1983; Zakharov and Zaslavskii, 1982; Young, 1993; Pushkarev et al., 2003; Resio et al. 2004, 2011; Badulin et al., 2005, 2007). Unfortunately, a primary difficulty implicit in models that incorporate S_{nl} into their net source-term balance is that, even with today's computer power, they must use approximations to the complete interaction integral rather than the complete integral itself (e.g. WAMDIG, 1988; Lin and Perrie, 1999; Jenkins and Phillips, 2001; Pushkarev et al., 2004; Tolman, 2013).

As shown by Resio and Perrie (2008), the initial operational approximation for S_{nl} is the DIA, the discrete interaction approximation, which is still the primary form used by operational models today, cannot reproduce accurate frequency–direction estimates of S_{nl}. Instead, the DIA approximation is only calibrated to produce an approximate estimate of the total energy transfer to frequencies lower than the spectral peak frequency. Consequently, this source term cannot produce accurate estimates of energy and momentum fluxes through the spectrum for the entire range of wave growth as needed for coupled models.

Past comparisons of directionally-integrated and directional spectra produced by models to observations have been mainly conducted within a somewhat qualitative framework in which modeled and observed spectra are plotted either on the same graph or on adjacent graphs and discussed in terms of qualitative differences. An encouraging exception to this can be found in Alves and Banner (2003) who introduce some clear quantitative metrics for spectral comparisons in idealized fetch-limited wave growth. It has proven difficult to build a clear consensus on the accuracy of modeled wave spectra based on all of the qualitative comparisons shown in individual studies; so it appears that an alternative approach more along the lines of that introduced by Alves and Banner (2003) and complemented by Banner and Morrison (2010) may offer a much improved, generalizable method for evaluating the ability of wave models to produce accurate wave spectra.

The purpose of this paper is threefold. First, we will develop a set of observed spectral characteristics as potential metrics for spectral shape predictions using detailed-balance source terms in place of the current reliance on integrated parameter comparisons. Second, we will explore fundamental reasons why the existing operational approximation for S_{nl} cannot represent detailed balances in nonlinear transfers which control critical fluxes of energy, action and momentum through wave spectra. And, third, we will discuss the need to utilize phase-resolving information from ongoing direct numerical simulations to help formulate future phase-averaged source terms.

2. Detailed observations of spectral shape and their physical implications

Spectral shapes in nature can often have very complex forms containing several superposed wave trains, postulated to be the balance of three primary source terms: wind input (S_{in}), wave breaking (S_{ds}) and nonlinear interactions (S_{nl}) plus propagation effects. In situations with highly variable wind speeds and directions, the overall detailed balance among these three source terms and propagation effects can be very difficult to conceptualize and to quantify. For this reason, researchers have often used stratified samples, representing somewhat simpler, idealized conditions, as the basis of their analyses. A typical approach to this stratification has been to limit the sample to conditions of relatively constant wind speed and direction and in which only a single dominant spectral peak is evident (Toba, 1972, 1973; Hasselmann et al., 1973; Donelan et al., 1985; Resio et al., 2004; Ewans and Kibblewhite, 1990; Ewans, 1998; Long and Resio, 2007). Data of this type provides a good starting point for understanding the detailed shape characteristics of spectra and, in turn, quantifying the associated fluxes of action, energy and momentum through wave spectra. Since third-generation models were first operationalized (WAMDIG, 1988), a large amount of detailed measurements of wave spectra has been added to our knowledge base. This data provides a critical basis for improved understanding of detailed-balance physics and for evaluating the ability of detailed-balance wave models to reproduce accurate spectral shapes. In this section, we will review observed characteristics of wave spectra, beginning with analyses of directionally integrated spectral forms,

$$E(f) = \int_0^{2\pi} E(f,\theta)d\theta \tag{1}$$

where $E(f)$ is the directionally integrated spectral energy density as a function of frequency, f, $E(f,\theta)$ is the energy density of the directional spectrum as a function of frequency and propagation direction, θ. The shape of the directionally integrated spectrum tends to be related to net balances of energy and action, since these are scalar quantities which typically do not depend strongly on the directional characteristics of the spectrum. Following the section on directionally-integrated spectral metrics, we will examine observational characteristics of directional wave spectra. In this case, the spectral shape characteristics are expected to be strongly influenced by the balance of momentum among the source terms due to the vector nature of such fluxes, since they are a function of propagation direction.

2.1. Directionally integrated characteristics of wave spectra as spectral metrics

2.1.1. The equilibrium range

Data analyses are typically influenced by the physics paradigm held by those performing the analyses. Two different paradigms for directionally integrated spectral shapes have evolved from the 1950s to the present. In the 1950s and 1960s, wave spectra were believed to represent a direct balance between wind input and wave breaking. Thus, the spectral shape was postulated to transition toward a

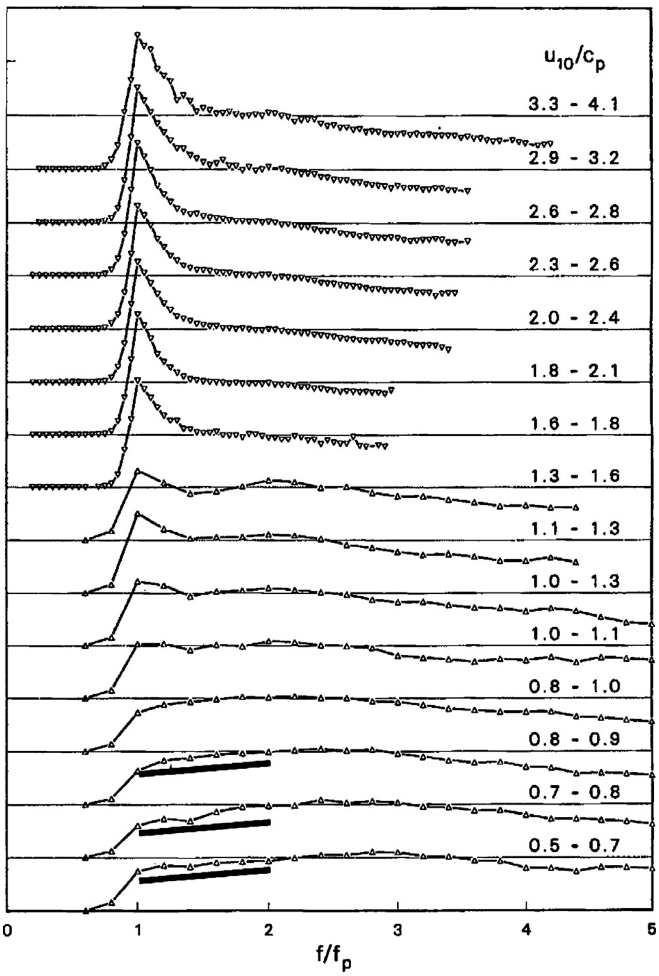

Fig. 1. Average compensated spectra [$\hat{E}(f) = E(f)f^4$] as a function of inverse wave age, wind speed divided by the phase speed of the spectral peak from Long and Resio (2007). A horizontal line denotes an f^{-4} form and the bottom three plots include heavy black lines at a compensated slope of $f^{-11/3}$ offset from the data, so the data are still visible.

dimensional form consistent with limitations on energy levels related to wave breaking in a spectral subrange of frequencies above the spectra peak, producing spectral shapes with a dimensional form $E(f){\sim}g^2f^{-5}$ (Phillips, 1958; Pierson and Moskowitz, 1964; Hasselmann et al., 1973), where g is gravity. In Phillips' initial arguments for this spectral shape, he argued that wave breaking occurs on a much shorter time scale than wind input, thus the coefficient controlling the spectral energies was expected to be a universal constant, $E(f) = \frac{\alpha_5 g^2 f^{-5}}{(2\pi)^4}$, where $\alpha_5 = 0.0081$. The work of Mitsuyasu (1968) and JONSWAP (Hasselmann et al., 1973) presented clear evidence that $\alpha_5$was not a universal constant. Instead, it varied systematically with dimensionless combinations of other wave generation parameters, such as wind speed, peak frequency and total energy within the spectrum.

In the early 1970s, an alternative spectral form was formulated by Toba (1972, 1973), based on wind-speed scaling $E(f) \sim u_w g f^{-4}$, where u_w is the wind speed. Subsequent observational studies (Forristall, 1981; Donelan et al., 1985; Resio et al., 2004; Long and Resio, 2007) have shown strong support for the f^{-4} equilibrium range (Fig. 1), where the frequency spectra in this figure have been transformed to a compensated form via multiplication by f^4, i.e. $\hat{E}(f) = E(f)f^4$, where $\hat{E}(f)$ designates the compensated spectrum. As can be seen in results from Long and Resio (2007) in Fig. 1, which took particular care to limit the observations in their sample to relatively constant winds and situations with a single spectral peak, the compensated spectral shapes from many sites around the world exhibit a remarkably consistent f^{-4} form in their equilibrium ranges, although it can be seen that the extent of the equilibrium range varies as a function of wave age. Thus, the first metric proposed here is the ability of detailed-balance physics in a wave model to maintain a clear f^{-4} form throughout an appropriate equilibrium range as determined by detailed analyses and observations. This metric provides an important constraint on all three primary source terms within this portion of the spectrum.

A dimensionally consistent form of an f^{-4} wave spectrum can be written as

$$E(f) = \alpha_4 u_a g f^{-4} \Psi_4(f_r) \tag{2}$$

where α_4 is a dimensionless coefficient, u_a is a physical constant with units of velocity, g is gravity, and $\Psi_4(f_r)$ is a dimensionless shape function of relative frequency $f_r = \frac{f}{f_p}$. Rewriting the f^{-5} spectrum into a comparable form yields

$$E(f) = \alpha_5 g^2 f^{-5} \Psi_5(f_r) \tag{3}$$

with the subscripted terms in Eq. (3) playing analogous roles to the f^{-4} form in Eq. (2).

In Toba's (1972) original formulation, it was hypothesized that this u_a in Eq. (2) represented the wind speed, since this provided the correct dimensional units; however, Resio et al. (2004), following up on early work by Resio and Perrie (1989), postulated that a more suitable physical representation of this term might be $u_a = (u_w^2 c_p)^{1/3}$, where u_w is the wind speed and $c_p$is the phase speed of the spectral peak. Figs. 2 and 3 show the relationships between energy levels in the equilibrium range plotted against u_w and against $(u_w^2 c_p)^{1/3}$, respectively. Clearly, the more consistent representation comes from the latter scaling for energy levels in the equilibrium range.

As shown by Resio et al. (2004), energy fluxes through the equilibrium range due to nonlinear interactions have the form

$$\Gamma_E^+ = Z\frac{u_a^3}{g} \tag{4}$$

where Z is a dimensionless constant, which depends weakly on directional spreading. For the case of u_a=u_w, Eq. (4) might be interpreted as implying a constant energy transfer rate into the wave field from the atmosphere during the wave generation process for constant wind speed and direction. For the case of $u_a = (u_w^2 c_p)^{1/3}$, Eq. (4) implies a constant momentum transfer rate into the wave field from the atmosphere during the wave generation process (Resio et al., 2011). The latter interpretation is also consistent with discussions of overall energy and momentum balances discussed in Hasselmann et al. (1973) and was developed in more detail in Resio and Perrie (1989), who noted that a constant rate of momentum transfer to, and retention within, the wave field is also consistent with the observed linear growth of total wave energy with fetch. Thus, the second metric, or in other words, the second spectral shape characteristic selected for evaluating detailed-balance source terms is their ability to reproduce the relationship between specific relation between the energy levels in the spectral equilibrium range for constant wind speeds and a wind speed metric, i.e. it should approximate the βvs.u_a relationship shown in Fig. 3, where β here is the deep-water version of the equilibrium range energy constant as defined in Resio et al. (2004), i.e. $\beta = \frac{1}{n_1 - n_2 + 1}\sum_{n_1}^{n_2} f^4 E(f)$. This will help establish quantitative limits on the magnitudes of the wind input and wave breaking source terms that act as a combined source for these fluxes during the wave generation process. As an initial approximation, $n_1$andn_2 will be assumed to limit the range used to estimate β to $1.5f_p - 3.0f_p$, consistent with Resio et al. (2004).

2.1.2. Spectral peakedness

Compensated spectra in Fig. 1 show that there is a region of the spectrum with elevated energies in the vicinity of the spectral peak,

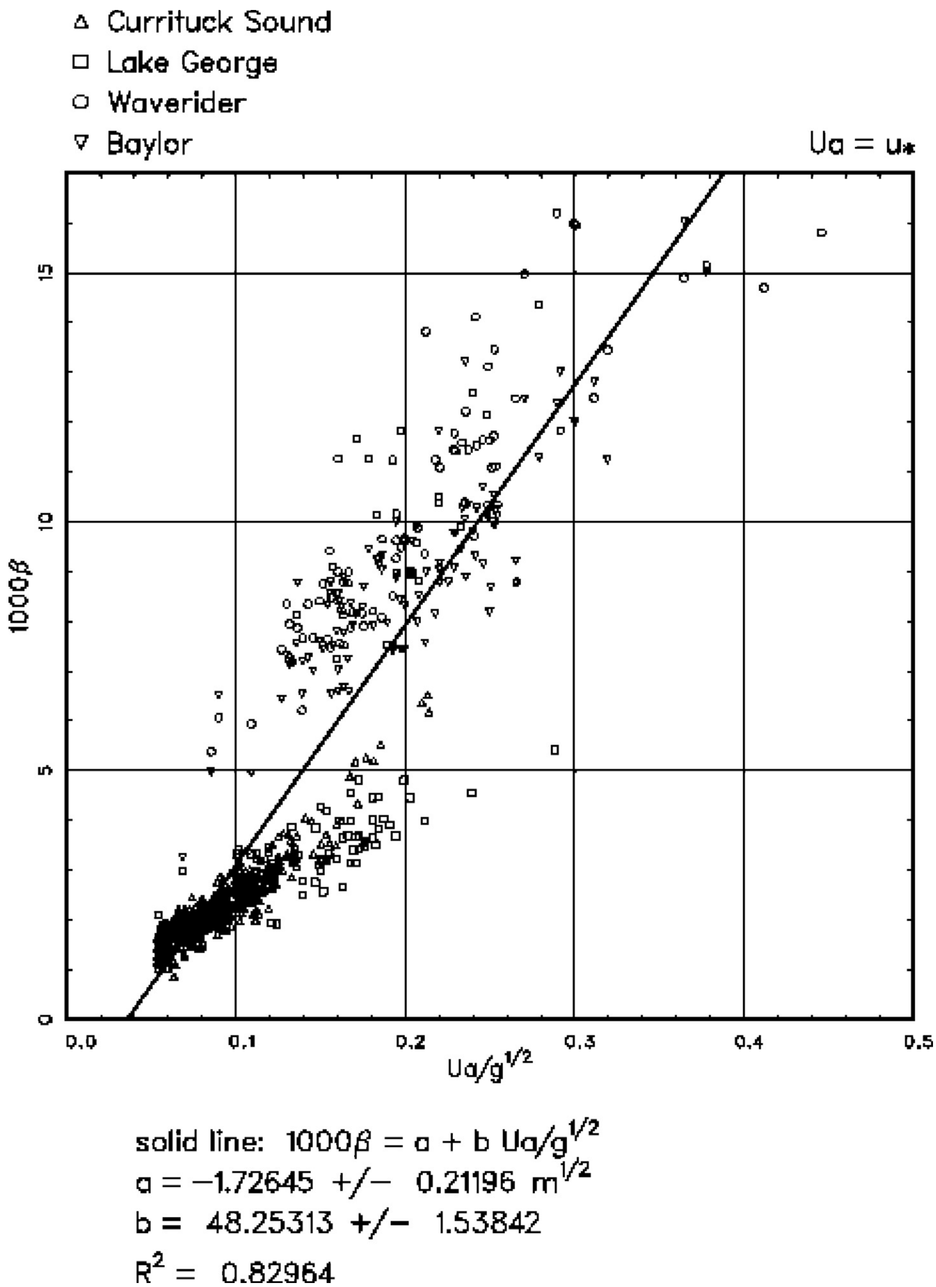

Fig. 2. Equilibrium range coefficient as a function of wind speed for different sites around the world from Resio et al. (2004). The slope of the lines from different locations do not connect into a single-valued function.

Table 1
Equivalent peakedness values for JONSWAP (γ) and f^{-4}–based(γ_r) spectral shapes.

γ_r	4.32	3.09	2.04	1.23	0.62
γ	7	5	3.3	2	1

with the peakedness most pronounced at low wave ages and diminishing as wave age increases, where wave age is defined as the phase speed of the spectral peak, c_p divided by the wind speed, u_w. Consistent with the arguments by Resio et al. (2004), it is deemed advantageous to move from an f^{-5} basis to an f^{-4} basis for consistency with the new equilibrium range form, rather than retaining the JONSWAP (f^{-5}) basis for the definition of peakedness. Table 1 provides a comparison of peakedness values for each of these classes of spectra.

Fig. 1 shows that, although spectral peakedness does exhibit a relatively high scatter, the average characteristics follow a consistent pattern, with a tendency for high peakedness in young waves (small values of c_p/u_w) diminishing to lower peakedness as wave age increases. Observational evidence from Romero and Melville (2010) supports this same trend, albeit with slightly varied values. Thus, the third metric, viz. the third spectral characteristic, for evaluating detailed balance source terms is their ability to match the approximate peakedness behavior shown in Fig. 1. This constrains the source term balance by requiring that it have the ability to create higher peakedness in young waves, even though the total momentum passing through the equilibrium range may be hypothetically transferring a relatively constant amount of momentum out of the spectral peak region through the equilibrium range.

2.1.3. Transition from an f^{-4} to an f^{-5} form at high frequencies

Forristall (1981) noted, in an analysis of a large data set from the Gulf of Mexico, that wave spectra transitioned from an f^{-4}

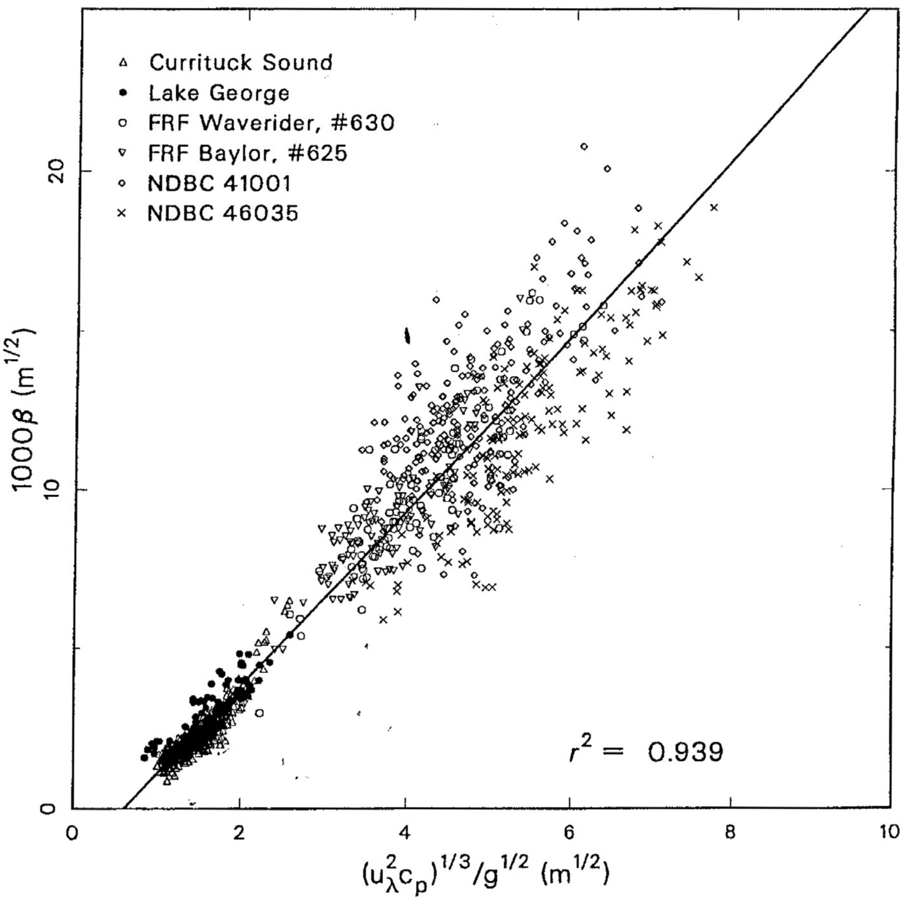

Fig. 3. Equilibrium range coefficient as a function of the cube root of wind speed squared times the phase velocity of the spectral peak for different sites around the world from Resio et al. (2004). The slope of the lines from different locations connect into a single-valued function. As defined in Resio et al. (2004), the reference wind speed (u_λ) in this figure is the wind speed at Miles critical layer height above the mean water level.

equilibrium range to an f^{-5} equilibrium form at a frequency which depended on wind speed. It has long been recognized that local wave steepness exceeds its allowable theoretical limit if the f^{-4} spectrum is allowed to extend to very high frequencies. The data in Fig. 4 suggests that this transition depends on wave age which, in turn, implies a dependence on spectral peakedness. Data from Romero (2008) is presented in terms of inverse wave age using friction velocity ($\frac{c_p}{u_*}$) and also shows a pronounced tendency for this transition to progress from low values of relative frequency in wave spectra, for young waves, to larger values of relative frequency as wave age increases. As an interesting note here, very short-fetch studies such as some of the Currituck Sound data and data from a reservoir collected by Birch and Ewing (1986) show that, in cases for which the inverse wave age is greater than 7 or so, the f^{-5} form approaches the spectral peak so closely that there is little or no f^{-4} equilibrium range. Their data, as well as some of the data from Currituck Sound (Long and Resio, 2007) shows that this transition occurs in very young waves occurs around 1.4 f_p; whereas the highest values of inverse wave age in Fig. 1 has a mean value around 3.5 with a transition at $2f_p$. Thus, the fourth metric, or fourth evaluation criterion for detailed balance source terms, is their capability to reproduce variations in the transition frequency in a fashion consistent with Fig. 4. This metric has been used in modeling work by Romero and Melville (2010) and places strong constraints on the form and magnitude of the wave dissipation source term. Even though the exact pattern of change is still being developed, this metric provides a valuable constraint needed for estimating wind-wave momentum fluxes in this range.

2.1.4. Development of an $f^{-11/3}$ range in spectra with wave ages exceeding the "fully-developed" form

Ever since Pierson and Moskowitz (1964) provided extensive data for scaling wave spectra for which the phase speed of the waves at the spectral peak are approximately equal to one, it has been tacitly assumed in most wave models that the fully-developed spectral form developed by these researchers is a necessary test for a spectral wave model. However, theoretical analyses by Zakharov and Zaslavskii (1982) showed that a spectrum can continue to evolve toward a constant "action-flux" form in which the action flux from the region of wind input is directed toward lower frequencies. In this context, if the region of breaking in the spectral peak region does not form a zero balance at each frequency and angle with net energy gains from nonlinear transfers to lower frequencies, a spectrum would not be expected to evolve into an absolutely-stationary, fully-developed form. Although Komen et al. (1984) were able to achieve a "quasi-stationary" directionally integrated spectral form in their investigation into the existence of a fully developed wind-sea spectrum, they were not able to match the directional characteristics of the source terms to achieve absolute stationarity in a detailed-balance sense. Glazman (1994), in an investigation into wave spectra in the vicinity of Hawaii, concluded that a majority of open ocean observations yield wave age values and spectral exponents that disagree with the concept and shape of a fully-developed spectrum; thus, it is possible that the hypothesized "fully-developed spectrum" does not represent an end-state for spectral development. In Fig. 1, the spectra at wave ages exceeding 1 show a change in slope at the location within the spectrum at which the wave age approximately equals 1,

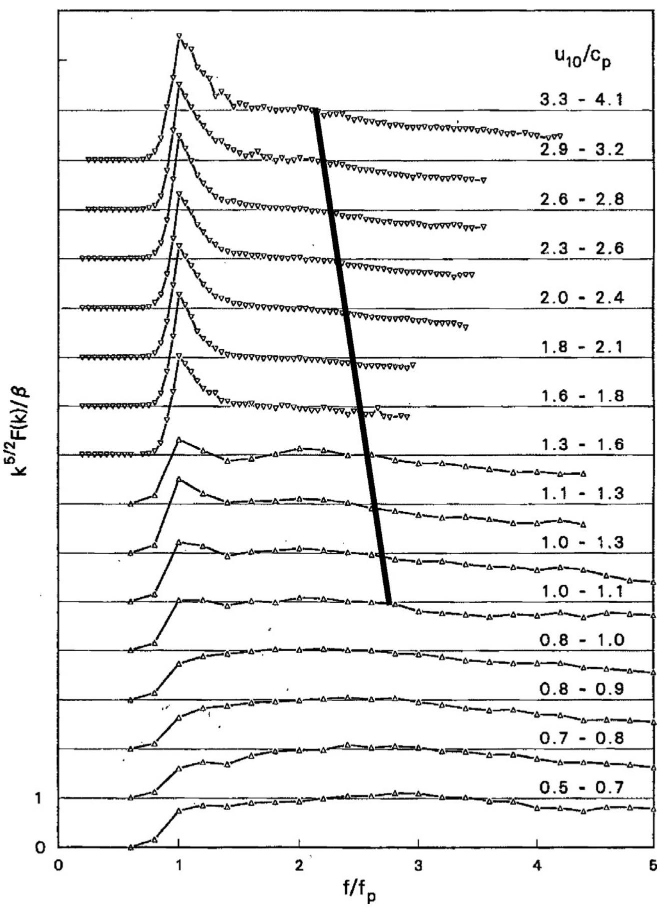

Fig. 4. Average compensated spectra in Fig. 1 with a line denoted the transition from an f^{-4} equilibrium range to an f^{-5} spectra range at relative frequencies which increase as the inverse wave age decreases. The line is limited to the range inverse wave ages ≥ 1.

consistent with the arguments of Glazman (1994), shown by offset lines with "compensated" slopes for an $f^{-11/3}$ spectral form. As seen here, the slope of the line in this region of the spectrum is very close to the theoretical form for a constant action flux toward low frequencies $E(f)\sim f^{-11/3}$, as qualitatively supported in the bottom four compensated spectra in Fig. 1.

Even though the spectral shape appears to continue to evolve past a single "fully-developed" form, observations suggest that the rate of gain of total energy in the spectrum asymptotically slows and may asymptotically actually approach zero (Walsh et al., 1988). This implies that the detailed-balance source terms act in a fashion that allows wave spectra to evolve past a fully-developed Pierson–Moskowitz spectral form while asymptotically reducing the rate of increase in total wave energy. The ability of a detailed-balance model to reproduce observed energy slopes in frequencies lower than the phase speed equal to the wind speed while asymptotically slowing the growth of wave energy will be taken here as the fifth metric for evaluating such models.

2.1.5. Relaxation to an equilibrium form

One of the original arguments of WAMDIG (1988) for adopting a detailed-balance form for all source terms in spectral wave models was to properly account for the relaxation of a spectrum from a perturbation toward its shape-stabilized, quasi-equilibrium form exhibited in Fig. 1. Thus, a necessary criterion for the detailed-balance source terms used in coupled model applications will be that these source terms produce a relaxation to the correct form at a quantitatively correct rate. Fig. 5 shows the relaxation rate of a perturbation superposed on a spectrum with an f^{-4} spectral form near full development from numerical simulations using the WRT integral for S_{nl} compared to results from the evolution using the DIA. The left-hand panel shows the evolution of the equilibrium using the DIA, while the right-hand panel shows the evolution from produced by the complete integral. It is interesting to note in this figure that the introduction of the transition to an f^{-5} form does produce a slight deviation from the f^{-4} form here; however, not the same magnitude of deviation as the DIA-force equilibrium. Since the ability of the source terms to force a spectrum toward an equilibrium is a critical requirement for detailed-balance models, this ability will be taken here as the sixth metric for evaluating detailed-balance source terms.

2.2. Directional characteristics of wind wave spectra

Directional spreading attributes of wind-wave spectra provide some additional information regarding the relative magnitudes of the different source terms, particularly in terms of their net momentum balance. All three of the source terms noted here have been characterized by different directional functions within wave models. The wind input in existing operational models is typically of a

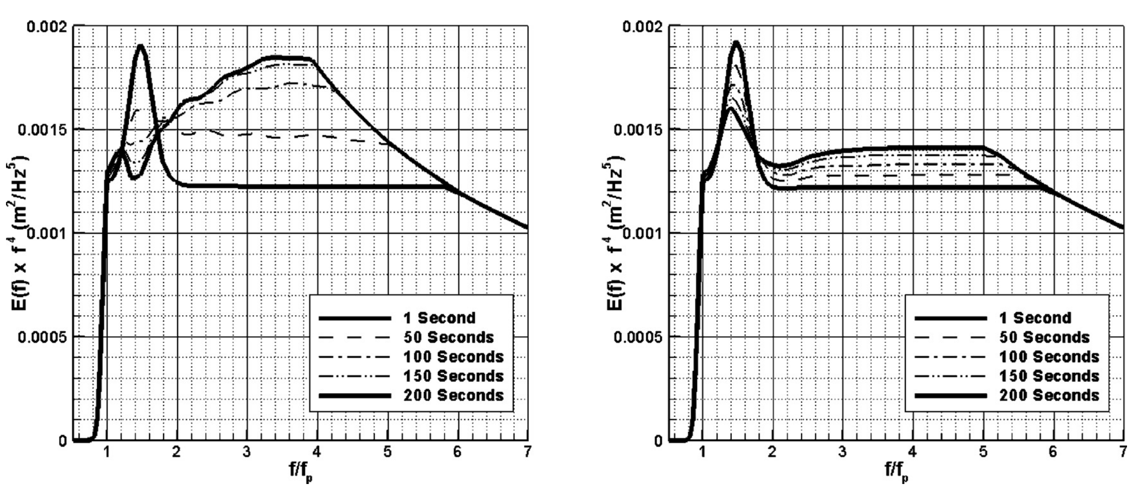

Fig. 5. The evolution of a spectrum perturbed from an initial f^{-4} form with a peak frequency at 0.3 Hz by the addition of a Gaussian-shaped "hump" of energy, based on four-wave interaction integral, with the left panel showing the evolution produced by the DIA and the right panel showing the evolution produced by the complete integral solution. In this example, the spectrum is constrained to follow an f^{-5} form at frequencies above a transition limit consistent with the spectra shown in Fig. 4. As can be seen here, the spectrum builds back toward an f^{-4} form relatively quickly on the high frequency side of the perturbation and much slower on the low frequency side.

$S_{in}(f,\theta)\sim S_{in}(f)\cos^n(\theta-\theta_0)$ form, where θ is the propagation direction and θ_0 is the wind direction. Breaking is usually considered to be proportional to the local energy, so it is usually characterized as having a form given by $S_{ds}(f,\theta)=S_{ds}(f)\phi(f,\theta)$, where $\phi(f,\theta)$ is the proportion of the energy in a given model angle band at frequency f. Some sets of second-generation source terms (Donelan et al., 2012) with alternative forms for the source term balance substantially reducing the role of S_{nl} can also achieve a general spectral form with increased directional spreading at frequencies higher than and lower than the spectral peak; however, the specific capabilities to match the quantitative characteristics included lobe ratios have not been tested. The combination of wind input and breaking alone do not produce functional behavior that either independently or in combination can produce angular spreading that is narrowest at the spectral peak and becomes broader at frequencies both higher and lower than the peak. On the other hand, the nonlinear flux energy of from the peak to higher and lower frequencies has been shown to have this signature; and as shown in Resio et al. (2011), the observed variation in angular spreading around the peak in several studies is consistent with the necessary spectral shape required to maintain constant momentum fluxes from the spectral peak region to higher and lower frequencies.

Besides the well-established pattern of increasing angular spreading as a function of increasing frequency difference from the spectral peak, there is a significant body of evidence (Young, 1995; Ewans, 1998; Wang and Hwang, 2001; Long and Resio, 2007; Romero, 2008; Romero and Melville, 2010) showing that directional spectra measured in relatively short experiments develop very pronounced bimodality and that such bimodality is directly linked to nonlinear energy and momentum exchanges in wave spectra (Tofolli et al., 2010). Wang and Hwang (2001) defined a term called the lobe ratio, which was a ratio of the average peak of the energy densities in the spectrum to the energy density at the mean propagation angle of the spectrum. Wang and Hwang defined two terms, an "angle separation" and a "lobe ratio." In their paper, they utilize a wavenumber basis since these spectra were measured in a spatial basis. Here, since wave models typically utilize a frequency–angle basis, we will use a frequency–angle form for our analyses. In shallow, variable-depth areas, the wavenumber basis may offer some benefits in terms of representing the effects of refraction, but that is not the focus of this paper.

In a frequency–direction basis, the angle separation and lobe ratio can be defined as

$$\theta_s(f)=\frac{\theta_1(f)+\theta_2(f)}{2}$$

and

$$r_{lobe}(f)=\frac{E(f,\theta_1)+E(f,\theta_2)}{2E(f,\bar{\theta})}$$

where $\theta_s(f)$ is the angle separation, which has been found to vary as a function of frequency, and $r_{lobe}(f)$ is the lobe ratio. The three angles are defined as follows: θ_1 and θ_2 are taken as the angles with the maximum energy on each side of the mean propagation angle and $\bar{\theta}(f)$ is the mean propagation angle at frequency f, i.e. $\tan^{-1}[E_y(f),E_x(f)]$ where

$$E_y(f)=\int_0^{2\pi}E(f,\theta)\sin(\theta)d\theta$$

and

$$E_x(f)=\int_0^{2\pi}E(f,\theta)\cos(\theta)d\theta.$$

Romero (2008) in an extensive analysis of bimodality (Fig. 6), which includes extensive data set from experiments in the Gulf of Tehuantepec, provided an excellent review of bimodality in wave spectra. He noted that early measurements from buoys (Mitsuyasu et al., 1975; Hasselmann et al., 1980) and the spatio-temporal measurements of Donelan et al. (1985) concluded that the angular distribution was unimodal; whereas spatial measurements (Cote et al., 1960; Holthuijsen, 1983; Hwang et al. 2000a, 2000b) have all concluded that the angular distribution in young waves is very bimodal. It can be noted that the data in Long and Resio (2007) are also from spatio-temporal measurements. Romero and Melville (2010) pointed out that studies by Benoit (1992) and Krogstad (1990) have shown the ability of a buoy to resolve multi-modality in wave spectra to be strongly affected by the method used to process the data.

In Romero's (2008) data compilation, he found that there was a clear relationship between wave age and the lobe ratio, with older waves being less bimodal. Resio et al. (2011) also shows a directional function in which increased spreading of the side lobes leads to reduced bimodality in the directional distribution as wave age increases. The low resolution of the early analysis methods used in analyzing directional spectra, particularly at high frequencies where these effects are most pronounced, combined with the tendency for open ocean wave spectra to be more representative of older wave ages may help explain the earlier interpretation of wave spreading in terms of unimodal spreading functions. In terms of quantitative effects there is a consensus that young (sort-fetch) wave spectra exhibit lobe ratios in excess of 2 even at relative frequencies in the range of 2–3. Toffoli et al., (2010) obtained similar lobe ratios using numerical simulations of the potential Euler equations, which compared well to their laboratory results of the development of bimodality from initially unidirectional spectra. Based on all this evidence, the ability of detailed-balance wave models must be to reproduce these high lobe ratios at the appropriate angles as the seventh metric for evaluation of detailed-balance models.

3. Estimation of nonlinear action, energy and momentum fluxes through a spectrum

As noted in the previous section, many of the attributes of spectral shape are consistent with expected characteristics associated with nonlinear fluxes of energy, action and momentum through wave spectra. For example, the f^{-4} equilibrium range is consistent with constant fluxes through this spectral region (Zakharov and Filonenko, 1966; Kitaigorodskii, 1983; Resio and Perrie, 1991). The observed variation of angular spreading as a function of relative frequency is consistent with the form required to maintain a constant momentum flux through the spectrum (Resio et al., 2011). The relationship between increased peakedness (decreased wave age) and the lobe ratio is consistent with the behavior of fluxes expected from nonlinear interaction (Tofolli et al., 2010). And, the generation of a constant action flux region at frequencies lower than the spectral peak in waves with wave ages exceeding 1 (spectral peak celerity exceeding the wind speed) is consistent with the expected form established by (Zakharov and Zaslavskii, 1982; Glazman, 1994).

The peakedness of the wind-wave spectra as a function of wave age is not well represented in spectral shapes produced by existing operational models, nor is the transition from f^{-4} to f^{-5} directionally-integrated forms represented in these models, except by subjective parametric constraints. These two characteristics of spectral shape cannot be understood in terms of only dominant nonlinear interactions; consequently, they provide valuable information to help us understand the quantitative balance between wind input, wave dissipation and wave–wave interactions in different parts of the spectrum. The two different concepts for wave breaking: (1) dominant breaking located primarily within the spectral peak region in young waves which transitions to more evenly distributed breaking with increasing wave age, and (2) dominant breaking restricted to intermediate to high frequencies, will likely produce very different peakedness behavior as a function of wave age. Likewise, the shift of the relative frequency at which the relatively sharp transition from f^{-4} to f^{-5} directionally-integrated forms occurs will provide a valuable constraint on the form and magnitude of the dissipation function.

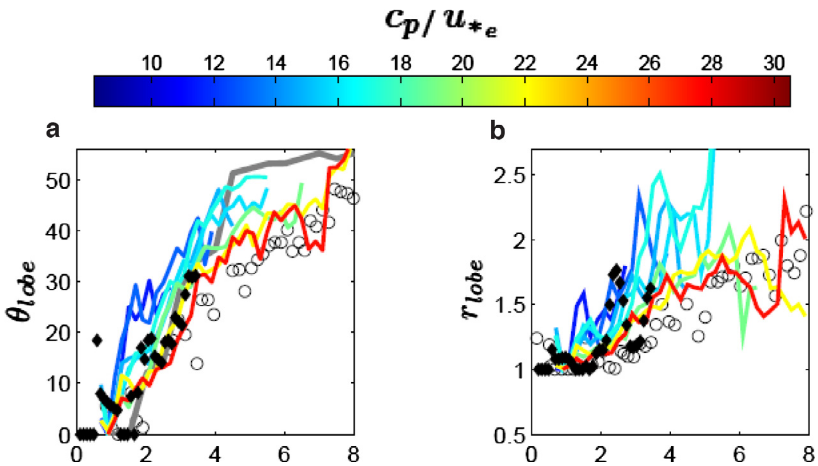

Fig. 6. Dependence of the lobe ratio determined in the Gulf of Tehauntepec (Romero, 2008) showing the existence of lobe ratios of about 2 at a relative wavenumber $k/k_p = 4$ in young waves and a systematic decrease in the lobe ratio as wave age increases.

3.1. Inconsistencies in current operational approximations to S_{nl}

Given the recognized importance of nonlinear interactions to the formation of characteristic spectral shapes and the body numerical results over the last decade confirming the validity of the Hasselmann (1962) equation for nonlinear transfers within a continuous spectrum (Tanaka, 2001a, 2001b, 2007; Korotkevich et al., 2007), it seems evident that an absolutely critical component of a detailed-balance wave model is for it to have an accurate representation of S_{nl} within it. However, as shown in Resio and Perrie (2008) for f^{-5} (JONSWAP) spectra for f^{-4} spectra, the approximation to S_{nl} for nonlinear interactions in existing wave models, based on the discrete interaction approximation (DIA) (WAMDIG, 1988), exhibits large systematic biases in its representation of the directionally-integrated form for S_{nl}. Whereas, it might be possible for a combination of additional source terms to compensate for such deviations in terms of integrated parameters, such compensation will distort the detailed-balances affecting fluxes through the spectrum and spectral shape.

Hasselmann's (1962) original derivation showed that four waves are required for permanent transfers of energy to take place within a continuous wind-wave spectrum. Estimation of the "exact" integral for these transfers has been approached in various manners and has been shown to be tractable in a number of studies (Webb, 1978; Masuda, 1980; Tracy and Resio, 1982; Resio and Perrie, 1991). As noted previously, computation of exact forms for S_{nl} remains beyond available computational resources for operational modeling. Early wave models attempted to overcome this problem by using parametric representations of this source term (Barnett, 1968; Ewing, 1971; Resio, 1981). However, Hasselmann et al. (1985) and WAMDIG (1988) argued that it was important to allow nonlinear interactions to contain as many degrees of freedom as the directional spectrum itself in order to form a consistent detailed-balance basis for this term. In fact, the distinction between parameterized representation of S_{nl} and the use of a representation for S_{nl} which retains the same number of degrees of freedom as the directional spectrum being modeled is the basic distinction between second-generation wave models and third-generation wave models.

After an examination of several alternatives, Hasselmann et al. (1985) proposed an approximation based on limiting the interactions to the integral form proposed by Phillips (1960) specifically for interactions among three waves. Problems with the DIA have previously been noted; and many papers have been written on the topic of either optimizing the DIA or extending it to a more generalized form (Tolman, 2013). It is clear from the methodology used to calibrate the DIA that it did not focus on the agreement between the

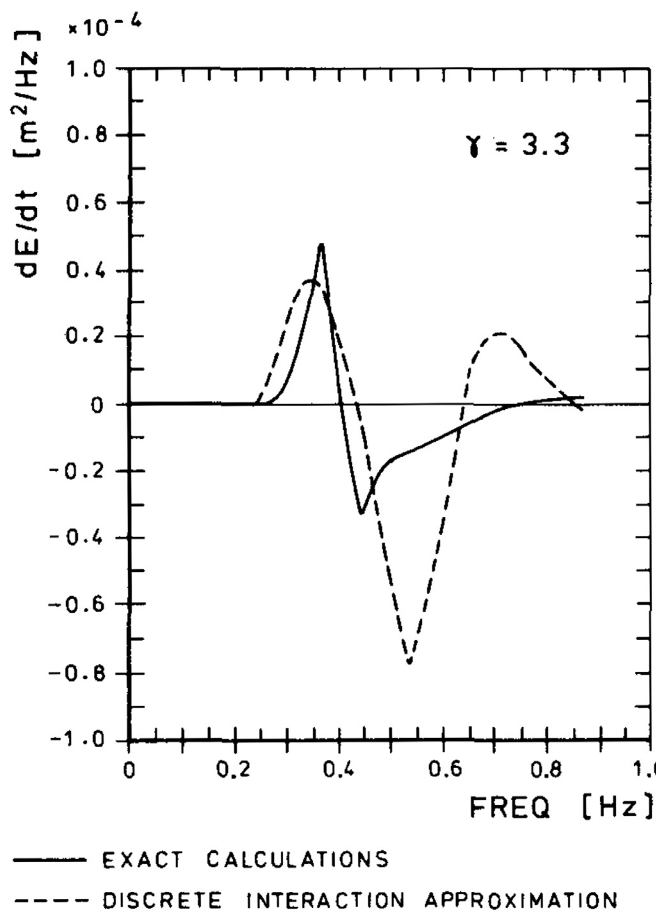

Fig. 7. The initial calibration of the discrete interaction approximation from Hasselmann et al. (1985). The metric used for goodness of fit of the approximation was the integrated transfer of energy to the frequencies lower than the spectral peak; thus, the negative deviation at frequencies above the spectral peak was not considered in the choosing calibration coefficient.

detailed shape characteristics of the new source term compared to the full integral representation. Instead, the calibration case reproduced here (Fig. 7) and its discussion, focused only on matching a parametric quantity, the total energy transferred into frequencies lower than that of the spectral peak. Thus, the DIA was developed specifically to be a detailed-balance source term for approximating

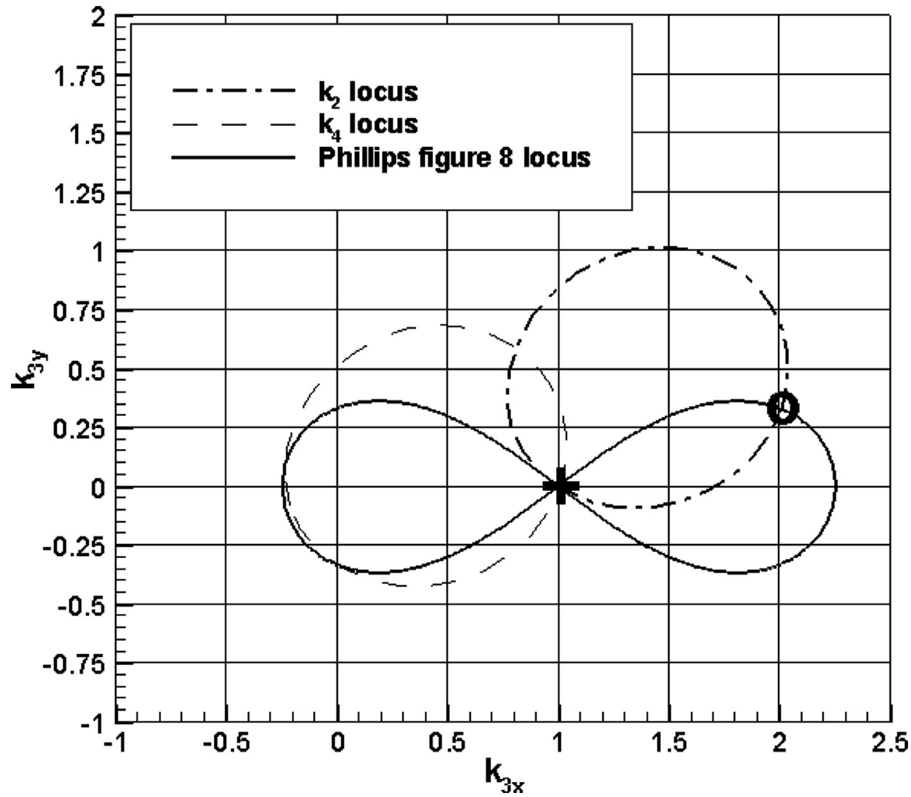

Fig. 8. Diagram showing the $\vec{k}_2$ and $\vec{k}_4$ loci for $\vec{k}_1 = (1, 0)$ and $\vec{k}_3 = (2.0, 0.26)$. The $\vec{k}_3$ point is selected to fall of the Phillps three-wave interaction locus with the center point of this three-wave locus falling at $\vec{k}_1$. The "+" at the $\vec{k}_1$ point is the one point where all interacting waves coincide for the case of self-interactions. The "O" represents the $\vec{k}_3$ point on the figure 8 is also a point on the $\vec{k}_2$ locus. Thus the four-wave interactions allow a point at $\vec{k}_3$ to interact with $\vec{k}_2$ points anywhere on the locus shown here.

integrated contributions of nonlinear interactions to wave growth and not for providing a detailed-balance representation of spectral shape, as evidenced by the large discrepancy in the frequency range immediately above the spectral peak. Although many studies have suggested that the DIA is based on an equivalent form of the full transfer integral; however, as will be shown here, there are dimensional, geometric and flux-related differences that cannot be tuned out of the reduced form for integral used as the basis for the DIA.

Using the transformation initially proposed by Webb (1978), the four-wave interaction form for S_{nl} can be written as

$$\frac{\partial n(\vec{k}_1)}{\partial t} = \int_{-\infty}^{\infty} \cdots \int_{-\infty}^{\infty} C^2 D^3 \delta\left(\sum_{i=1}^{4} q_i \vec{k}_i\right) \delta\left(\sum_{i=1}^{4} q_i \omega_i\right) dk_{2_x} \times dk_{2_y} dk_{3_x} dk_{3_y} dk_{4_x} dk_{4_y} \tag{5}$$

where $\vec{k}_i$ and ω_i represent the four interacting wavenumbers and radial frequencies for these waves, respectively; $q = 1$ if $i = 1$ or 2, and $q = -1$ if $i = 3$ or 4; C^2 is an algebraically complicated coupling coefficient which depends on all of the interacting wavenumbers; and D^3 is a sum of interacting triplets of action densities

$$D^3 = n_1 n_2 (n_3 + n_4) + n_3 n_4 (n_1 + n_2),$$

Removing the delta function on the wavenumber sum (by setting $\vec{k}_4 = \vec{k}_1 + \vec{k}_2 - \vec{k}_3$) and including the delta function on radial frequency (by restricting the integration domain to $\omega_2 = \omega_3 + \omega_4 - \omega_1$) allows this integral to be reduced to a form containing three dimensions in wavenumber space,

$$\frac{\partial n(\vec{k}_1)}{\partial t} = \int_{-\infty}^{\infty} \int_{-\infty}^{\infty} T(\vec{k}_1, \vec{k}_3) dk_{3_x} dk_{3_y} \tag{6}$$

as shown by Webb (1978), in which two of the three dimensions emerge explicitly in terms of $dk_{3_x} dk_{3_y}$. As shown by Webb (1978), the action transfer integral between $\vec{k}_1$ and $\vec{k}_3$, $T(\vec{k}_1, \vec{k}_3)$, represents a contour integral in which the integration around the contour provides the third wavenumber dimension,

$$T(\vec{k}_1, \vec{k}_3) = \oint C^2 D^3 |\partial W / \partial n|^{(-1)} ds. \tag{7}$$

Combining Eqs. (6) and (7) shows that the resonant four-wave interaction loci encompass a phase volume made up of a continuum of points in $k_{3_x} - k_{3_y}$ space surrounding $\vec{k}_1$ and a third dimension s along the resonant locus for k_2, with a coupled locus for $\vec{k}_4$ obtained by displacement from k_2 by the vector $\vec{k}_3 - \vec{k}_1$. Thus, the conditions for resonance reduce the six-dimensional integral in Eq. (1) to an inherently three-dimensional volume of interacting waves in wavenumber space (k_{3_x}, k_{3_y}, s).

The DIA form introduces an additional delta function into Eq. (5), $\delta(\vec{k}_1 - \vec{k}_2)$, which was not in the original derivation by Hasselmann (1962), essentially recasting the four-wave interaction integral back into the three-wave interaction form derived by Phillips (1960). Consistent with the dimensionality of a vector delta function in wavenumber space (k^{-2}), the introduction of this delta function removes two powers of k from the nonlinear interaction equation and reduces the transfer domain from a three dimensional volume to a single line, the "figure 8" shaped locus derived by Phillips, (1960). Fig. 8 shows an example of a figure 8 form for three wave interactions for interacting wave numbers of $\vec{k}_1 = (1,0)$ and $\vec{k}_3 = (2,0.3)$, along with the loci for $\vec{k}_2$ and $\vec{k}_4$ that satisfy the delta function on W. As can be seen in this figure, the figure 8 locus and the $\vec{k}_2$ locus intersect at only a single point. In fact, it can be shown that each point on the figure 8 represents only a single point on the $\vec{k}_2$ locus for each value of $\vec{k}_3$specified, thereby reducing the dimensionality of the integral from its original form.

Fig. 9 shows the three-wave interaction locus within the complete three-dimensional domain inherent in the full integral. In this

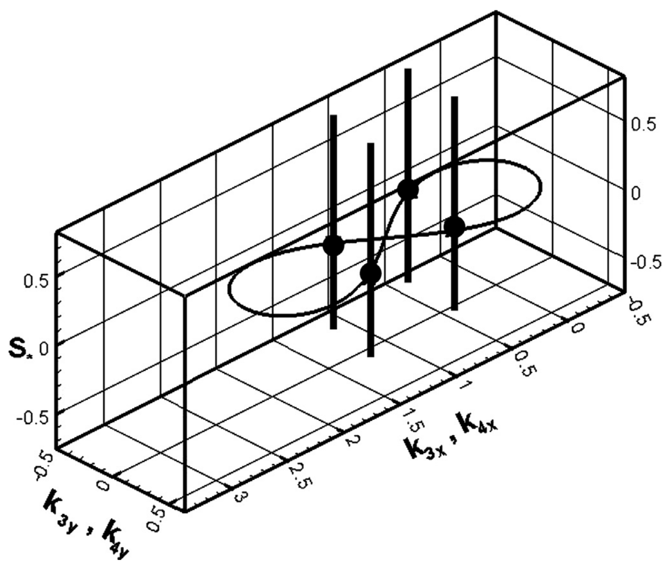

Fig. 9. The enclosed volume in the shape shown here illustrates the basic dimensions allowed for 4 wave interactions in the Webb (1978) form of the integral. Any $\vec{k}_3$ value is allowed in these interactions but the $\vec{k}_2$ values are constrained to lie along a locus such that $W = 0$ as described in the text, reducing it to a one-dimensional form, shown here as the vertical axis on this figure. In this figure the point where $\vec{k}_2 = \vec{k}_3$ is defined to be the zero referance point for s and the top and bottom of the box is recognized to the a branch cut across which the loci would connect continuously. The 4 points used in the DIA on the Phillips figure 8 diagram added here repesent individual points with no defined phase volume.

figure, the vertical axis represents the position along the locus s, with s_* defined such that the zero value coincides with the point along the locus at which the figure 8 pattern intersects with the locus. The four large dots in the figure represent 4 points along the locus taken as the quadruplet of points used by the DIA to approximate to the complete interaction integral. The four vertical lines in this figure intersecting with the quadruplets illustrate the point that the DIA approximation to the interaction includes only a selected point along the s dimension; rather than all the interactions along the locus, as well as only singular points in the k_{3_x}, k_{3_y} plane. Given the dimension of Eq. (5), it is clear that, if no singularities exist within the integrands in Eqs. (6) and (7), there can be no resonant transfers of action, energy, or momentum since the volume of the 4-point interaction integration domain included in Fig. 9 is zero.

To compensate for this dimensional inconsistency, a dimensional scaling function, B, was introduced into the formulation of the DIA, making their final form for the discrete interaction approximation, or DIA, (WAMDIG, 1988)

$$\begin{pmatrix} \delta N_1 \\ \delta N_2 \\ \delta N_3 \\ \delta N_4 \end{pmatrix} = \begin{pmatrix} -1 \\ -1 \\ +1 \\ +1 \end{pmatrix} B\hat{C}D^3 \Delta k_x \Delta k_y \Delta t \tag{8}$$

where N_i is the ith discrete increment of wave action in wavenumber space, $\hat{C}$ is a dimensionless coefficient used for tuning the approximation to match results from the full integral and D^3 is a term containing the triplets of action densities involved in the interactions at the quadruplets (Hasselmann and Hasselmann, 1985). For dimensional consistency, B had to have units equal to $(f^{19}g^{-8})$, given that the action densities in the triplets had f^{-5} directionally integrated forms, as believed under the paradigm for spectral shape at that time. Using Eq. (8) it is straightforward to show that the DIA-generated energy fluxes will become constant when

$$B[n(\vec{k})]^3 k^{3/2} \to [n(\vec{k})]^3 k^{11} \to \text{constant}.$$

In terms of a directionally integrated wave action ($n(k) = F(k)\omega^{-1}$, where n is wave action and F is wave energy as function of wavenumber and ω is radial frequency, $\omega = 2\pi f$) density spectrum the equilibrium range produced by such interactions would be of the form

$$n(k) \sim k^{-11/3}$$

For the directionally integrated equilibrium range energy density forms in wavenumber space, this gives

$$F(k) \sim k^{-13/6}$$

and for such a spectrum in frequency space, this yields

$$E(f) \sim f^{-10/3}$$

which, unfortunately, deviates significantly from the f^{-4} form for constant energy-fluxes implicit in the full integral. Thus, such a formulation cannot be used to estimate realistic fluxes through wave spectra. Detailed-balance simulations in Badulin et al. (2005) confirm that the energy fluxes lead to a pronounced deviation away from an initial f^{-4} form toward an $f^{-11/3}$ form and that the associated momentum fluxes also deviate significantly from the full integral representation for S_{nl}. As shown earlier in Fig. 5, the DIA forces the spectral shape significantly away from its recognized equilibrium form.

4. Improving source terms via phase-resolving models

A fundamental tenet of spectral wave modeling has been the assumption that a Fourier transform of the sea surface produces, with appropriate smoothing, a spectral approximation to our theoretical concept of a continuous wave spectrum. Reconstructions of individual water surfaces are typically made by inverse Fourier transform of the continuous spectrum with random phases under the assumption that the components follow linear wave theory. The source terms and propagation of energy in the model are then performed on the spectral components and added linearly to get the net water surface and associated characteristics.

Models of the three dimensional, time dependent sea surface incorporating nonlinearities to different orders have been developed to address situations where a linear reconstruction is inadequate. Examples include the higher order spectral models (HOS) (Dommermuth and Yue, 1987; Tanaka, 2001a, 2001b, 2007), broad-band nonlinear Schrodinger (BNLS) (Dysthe, 1979; Trulsen and Dysthe 1996), VORTWAVE (Nwogu, 2009) and the nonlinear flow analysis code (NFA) (O'Shea et al., 2008). Because these approaches resolve the surface waves in physical space, they are termed phase-resolved models to contrast to the phase-averaged spectral models. Xaio et al. (2013) demonstrate that the HOS model can (1) simulate the evolution of kurtosis, (2) reproduce the distribution of surfaces elevations and (3) develop and maintain a $k^{-5/2}$ equilibrium range consistent with laboratory and field observations. Xaio et al. (2013) compared the HOS and BMNLS driven by an initial Gaussian shaped spectrum. When the output of both models is Fourier transformed into spectra, both develop a peaked, JONSWAP-like omnidirectional spectrum with the expected $k^{-5/2}$ equilibrium range, noting that the JONSWAP spectrum in the equilibrium range appears very similar to a $k^{-5/2}$ equilibrium range due to the additional exponential function in its formulation. The directional spectra evolved from Gaussian to a bimodal directional distribution in the equilibrium range consistent with theory and observation (Long and Resio, 2007).

Combinations of Large-Eddy simulation (LES) models of the atmosphere and ocean coupled to realistic phase resolved sea states have been developed to investigate the interaction of the wave field with the two fluids. Sullivan et al. (2000, 2004), Lin et al. (2008), and Yang and Shen (2010) coupled a phase-resolved moving wave surface to an LES model of the atmospheric boundary layer and simulated a range of wave fields to study airflow over the waves and resulting profiles of boundary layer quantities. Sullivan et al. (2014) performed simulations corresponding to wave ages observed in the HiRES experiment

(Grare et al., 2013) varying from swell dominated to wind equilibrium cases and determined that fundamental characteristics of the lower boundary layer for near equilibrium conditions found excellent correspondence to Monin–Obukov theory. Yet for fast swell, the profiles deviated from traditional Monin–Obukov.

Yang and Shen (2010 , 2011) perform direct numerical simulation (DNS) and LES modeling of the lower atmosphere with an explicit atmospheric pressure terms so that the wave field can grow under action of the wind and show that both their LES and DNS models produce temporal growth rates consistent with field observations. Yang and Shen (2011) show that their wind-driven coupled model produces increased energies in the higher frequencies (and correspondingly rougher wave surfaces) than the unforced case (i.e. in the case of swell). Nwogu (2009), Brucker et al. (2010), Liu et al. (2013), Hu et al. (2012), Xaio et al. (2013), and Dommermuth et al. (2013) have approximations or direct calculation of breaking of individual waves which, when analyzed spectrally, appear to produce equilibrium ranges of the $k^{-5/2}$ to k^{-3} type found naturally. Similarly the LES and DNS formulations of the wave–ocean part of the problem have been developed (see for example, Brucker et al., 2010; Liu et al., 2013) that are effectively coupling the air–wave–ocean system at LES and DNS scales.

The foregoing sampling of results suggest that modeling the coupled air–wave–ocean system in physical space (as opposed to spectral space) is reaching a level of maturity where the principal mechanisms of wave growth, evolution and dissipation can be simulated directly along with their effects upon the air above and ocean below. It therefore becomes possible in principle to directly simulate the growth of wave fields with the feedback to the atmosphere and ocean and analyze the results in Fourier space. As this capability evolves, we should be able to contrast the growth and evolution of the wave field in physical space with our approximations in (phase-averaged) spectral space. This should allow addressing fundamental questions such as: (1) is the atmospheric input to a steep wave form calculated in physical space well approximated by linearized inputs to its spectral components, (2) is the loss of energy from a steep wave breaking in physical space well modeled by dissipation functions applied to its linear spectral components, and (3) does the sporadic time-space occurrence of input and dissipation average to the continuum spectral assumptions?

From the previous section, it is clear that the existing operational approximation for S_{nl} does not provide an accurate detailed-balance representation for energy and momentum fluxes and that flux divergence responsible for the relaxation from a perturbation toward a self-similar form will also deviate substantially from the full integral representation. Thus, it does not seem advisable to rely on test results which incorporate the DIA when attempting to develop improved detail-balance physics. In this section we will examine some implications of the observed spectral shapes, utilizing the full integral representation for S_{nl}.

As noted in the introduction to this paper, there is considerable controversy over the wave dissipation source term, S_{ds}, in terms of its role in different parts of the spectrum. Romero and Melville point out that present forms for energy dissipation due to wave breaking are based on heuristic physical arguments (Hasselmann, 1974) and are tuned via a number of free parameters to achieve agreement with observations (Komen et al., 1984; Banner and Young, 1994; Alves and Banner, 2003). Subsequent investigations (van der Westheysen et al., 2007; Ardhuin et al., 2010) have shown that these empirical fits are still a work in progress and do not appear to provide a general agreement to observations.

An alternative representation of wave breaking is found in Irisov and Voronovich (2010), who investigate the physical cause of wave breaking using an extension of the theoretical work of Longuet-Higgins and Cokelet (1976). Details of their numerical methods can be found in Irisov and Voronovich (2010) and will not be repeated here. Their fundamental results show that instabilities in wave fields develop in relatively short waves as they are "stretched and "squeezed" by longer waves or, as termed by Longuet-Higgins (1988), the "concertina effect". Monte Carlo simulations show that instabilities leading to wave breaking tend to be generated in the vicinity of the location of maximum current convergence. Wave breaking associated with such instabilities tends to occur slightly in front of or at the crest of large waves (Fig. 10). An interesting attribute of this breaking mechanism is that it is very sensitive to exceedance of a dynamic breaking threshold at the frequency at which the breaking occurs. Fig. 11 shows the dependence of the mean breaking frequency vs. the rms current gradient, where the breaking frequency was defined as the ensemble average of the time from an initial random phase start to breaking. These results imply a strong sensitivity of breaking to the rms variation in the superposed horizontal components of the wave orbital motions.

To adapt this concept to the onset of strong breaking in a phase-averaged spectral model, we assume that the horizontal wave velocities contributing to the breaking can be written as the sum of random phases combining to produce a horizontal current in the x-direction which exceeds a threshold related to $(\partial u/\partial x)^2$ which has dimensions of $(time)^{-2}$. Since we are interested in the ratio of this transition frequency to the peak frequency, we make this dimensionless by multiplying by f_p^2, yielding a dimensionless scaling function $P = (\partial u/\partial x)^2 f_p^2$. The $(\partial u/\partial x)^2$ term can be estimated by summing all the squared gradient of the x-components of motion of individual spectral elements, similar to any sum of variances. Each individual element will contribute a velocity gradient squared equal to $(agk\omega^{-1})^2$. Using the deep-water dispersion relationship and recognizing that $a^2 = E(f,\theta)\delta f\delta\theta$, this can be written as

$$P = f_p^2\left\langle\left(\frac{\partial u}{\partial x}\right)^2\right\rangle = f_p^2\int_0^{\lambda f_p}\int_{-\pi/2}^{+\pi/2}\left\langle\left(\frac{\partial u}{\partial x}\right)^2\right\rangle_{f,\theta} d\theta df$$
$$= f_p^2\int_0^{\lambda f_p}\int_{-\pi/2}^{+\pi/2} E(f,\theta)\cos\theta\,\frac{\omega^6}{g^2}d\theta df \tag{9}$$

where λ is the ratio of the frequency at which this term becomes sufficiently large to induce breaking sufficiently large that it forces the spectrum into an f^{-5} form and the subscripts "f,θ" denote the conversion to a contribution to the total velocity per unit frequency and angle increment. If we assume that the spectrum is of an f^{-4} form and is self-similar, Eq. (9) can be integrated analytically, yielding a relationship between the dimensionless value P and the integral in the second line of this equation,

$$P = \frac{\hat{\beta}\Phi_1(\gamma_r)\Phi_2(\sigma_\theta)\lambda^3}{gf_p} \tag{10}$$

where $\hat{\beta}$ is the equilibrium range scaling coefficient with units of velocity (where $\hat{\beta}$ denotes that the value of β is estimated from the data in a specific spectrums specific limits), $\Phi_1(\gamma_r)$ is a dimensionless, increasing function of peakedness and $\Phi_2(\sigma_\theta)$ is a dimensionless function of the angular spreading width. Since $\hat{\beta}$ has been shown to scale as a function of $u^{2/3}c_p^{1/3}$ (Fig. 3), Eq. (10) can be solved for λ as

$$\lambda \sim \frac{1}{(P\Phi_1(\gamma_r)\Phi_2(\sigma_\theta))^{1/3}}\hat{f}_p^{-2/9} \tag{11}$$

where $\hat{f}_p$ is dimensionless frequencey, defined as $\hat{f} = \frac{f_p u}{g} = \frac{u}{2\pi c_p}$. The impact of variations in angular spreading is not expected to play a major role in Eq. (11); however, decreasing peakedness will contribute to an increase in λ as will an increase in wave age. Thus, the form of Eq. (11) is qualitatively consistent with a sharp transition from an f^{-4} form to an f^{-5} form at a relative frequency which increases with wave age.

The wind input source is another term which, in its current form, is quite heuristically based. It was initially developed in a somewhat

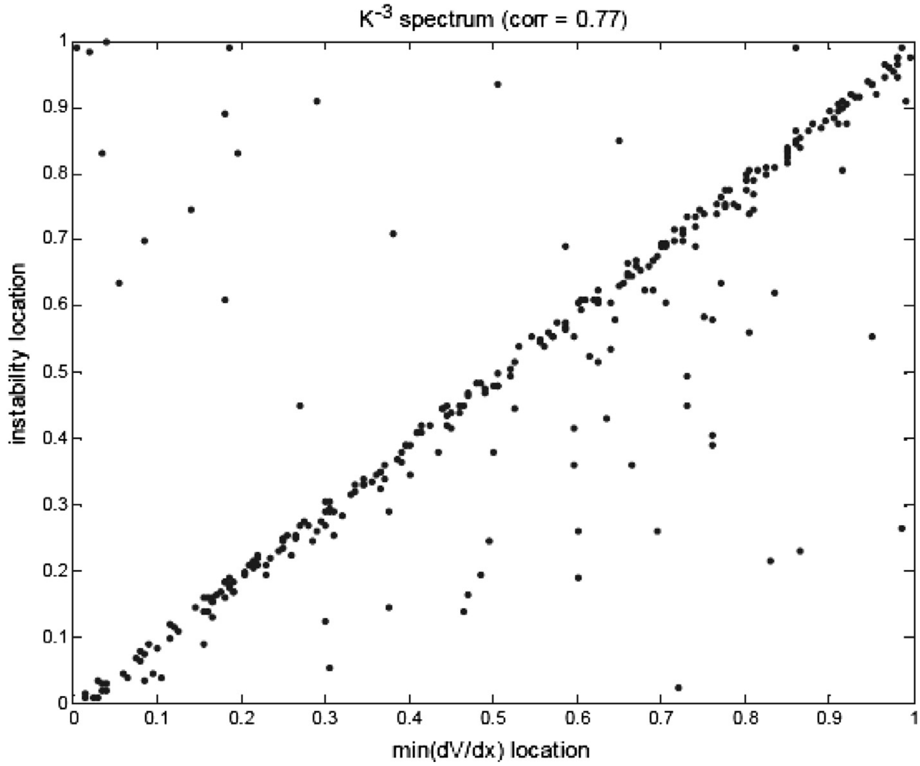

Fig. 10. The correlation of the point of incipient breaking in numerical simulations conducted by Irisov and Voronovich (2010) as a function of the point of strongest current convergence.

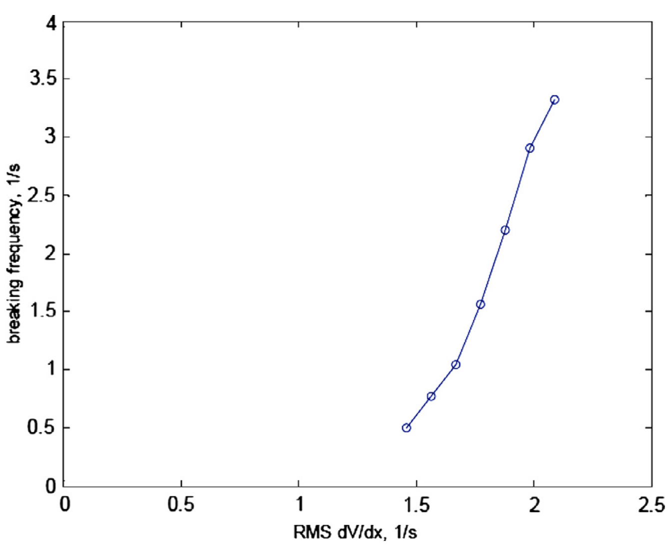

Fig. 11. Dependence of the mean breaking frequency on the mean surface current (negative) gradient as calculated in simulations by Irisov and Voronovich (2010).

rigorous manner for monochromatic, unidirectional waves (Miles, 1957, 1959), but was generalized to wave spectra under the assumption that individual spectral components each interacted independently with the winds above them, without any real justification for this assumption. Similar to the wave breaking source term, the tuning of various representations has been accomplished primarily via optimization within models (Komen et al., 1984; Tolman and Grumbine, 2013), accompanied by some heuristic arguments for the proposed modification. In fact, Tsagareli et al. (2010) showed that many of these proposed terms were not constrained by appropriate physical limits for total momentum transfer rates from the atmosphere into the water, leading to “remarkable disagreement both between the forms and also with the total stress measurement.” To compensate for these differences, he proposed a dynamic self-adjustment routine based on heuristic considerations and physical constraints.

Recent results of Sullivan et al. (2014), Yang and Shen (2010) and Yang et al. (2013) suggest that atmospheric flow patterns above a moving wave field interact with the moving water surface in a fashion that is not equivalent to the interaction with individual spectral components. Thus, similar to the wave breaking source term, detailed balance forms for wind input are still very much a work in progress. Also, similar to wave breaking, to capture key effects of wind-wave interactions, it appears that numerical experiments must be performed on a phase-resolving basis rather than on a phase-averaged basis. An ensemble of phase-resolving runs can then be used to estimate phase averaged source terms. Although much of the work in this area is still in its formative stage, results from such simulations should provide an improved basis for understanding and validating the detailed physics of source terms which could form the basis for a new generation of operational models which not only are tuned to produce good estimates of integrated wave parameters but which also produce improved spectral shapes and estimates of energy and momentum exchanges into and out of the wave field.

5. Conclusions

Operational wave models have made excellent progress since third-generation modeling began 30 years ago. What was a field of many independent, closed-source-code models with large discrepancies in their performance has evolved into a small number of mainly open-source models which enable effective collaboration among researchers around the world. This has led to a substantial effort toward developing wave models with global capabilities, at least in terms of predicting integrated wave parameters such as significant wave height, wave period and wave direction. Much of this work has been undertaken in a “holistic” approach, with free parameters in source terms adjusted to achieve best agreement with integrated parameters over large domains, rather than being driven primarily by physical arguments or detailed balance considerations. It is not clear that such testing provides a good basis for improving predictions of detailed characteristics of directional spectra, nor for estimating the energy and momentum exchanges that are needed for coupled modeling.

This paper presents a number of detailed spectral shape characteristics developed by researchers over the last 10–20 years. The argument is made here that such details provide a better basis for evaluating detailed-balance source terms in wave models than the continued use of integrated wave parameters. Many of the characteristics noted here are consistent with results expected in spectra dominated by fluxes produced by wave–wave interactions, such as the shape of the equilibrium range and the variation in angular spreading around the spectral peak. Others, such as the matching energy levels in the equilibrium range, variations in spectral peakedness and the transition from an f^{-4} form to an f^{-5} form at frequencies above the spectral peak, appear to require new detailed-balance wind and wave dissipation source terms in addition to an accurate representation of the nonlinear interaction source term.

The authors recognize that the choice of metrics to be used in detailed balance model evaluations will likely be a topic of considerable debate. However, for all the reasons noted here, we feel that it is essential to begin to move in this direction. This paper presents a number of detailed spectral shape characteristics developed by researchers over the last 10–20 years, which we believe should form an initial basis for these. Others may want to add to this list or modify/delete parts of this list; however, we feel that emerging needs in many areas make the development of such metrics important to many emerging applications in wind-wave modeling. The metrics suggested here include the ability of a model to reproduce the following spectral attributes:

1. an f^{-4} equilibrium range with an extent that depends on wave age,
2. a spectral peakedness defined in an f^{-4} context which depends on wave age,
3. an equilibrium range coefficient which is consistent with the momentum balance entering the wave field and passing through the equilibrium range,
4. a transition from f^{-4} to f^{-5} form at a location within the spectrum which varies as a function of wave age,
5. a relaxation from a perturbation that returns the spectrum to an appropriate equilibrium shape,
6. an evolution of a spectrum beyond the limit at which a fully-developed wave height is achieved, and
7. a bimodal directional distribution with the lobe angles and lobe ratios consistent with observations from spatio-temporal observations.

The argument is made here that many of the spectral attributes noted above appear to be closely related to spectral shape constraints created by nonlinear fluxes of action, energy and momentum through a wave spectrum. Our analyses show that the existing approximation for nonlinear interactions in operational wave models, which is based on a form for three-wave interactions, is inconsistent with the full integral for four-wave interactions. Other source terms can be tuned to roughly compensate for these inconsistencies in terms of integrated wave parameters in wave model testing; however, such tuning cannot reproduce the detailed balance form that controls the shape of the directional spectrum

We also note here that new concepts for detailed-balance source terms are beginning to emerge from phase-resolving spectral models and from direct numerical simulations. This work should lay a foundation for improved physics in spectral models; however, it is still essential to develop methods which can convert this progress into ensemble-averaged forms which can be utilized within operational models. As noted in the introduction, this progress may not lead to immediate improvements in terms of predictions of integrated wave parameters, but are urgently needed to meet emerging needs in remote sensing and coupled modeling.

Acknowledgments

Work conducted by Dr. Resio and Dorukhan Ardag on this material was supported by the National Ocean Partnership Program (NOPP), Award Number N00014-12-1-0127. The views expressed here do not necessarily reflect the views of this organization. The authors also wish to acknowledge the importance of contributions made by reviewers of this manuscript which extensively improved its content and readability. Finally, we would also like to thank Dr. Charles Long for his meticulous work on many of the data sets which contributed to this manuscript.

References

Alves, J.H.G.M., Greenslade, D.J.M., Banner, M.L., 2002. Impact of a saturation dependent dissipation source function on operational hindcasts of wind-waves in the Australian region. J. Atmos. Ocean Sci. 8 (4), 239–267.
Alves, J.H., Banner, M.L., 2003. Performance of a saturation-based dissipation-rate source term in modeling the fetch-limited evolution of wind waves. J. Phys. Oceanogr. 33, 1274–1298.
Ardhuin, F, Herbers, T.H.C., Watts, K.P., Vledder, G.P.V., Jensen, R., Graber, H., 2007. Swell and slanting-fetch effects on wind wave growth. J. Phys. Oceanogr. 37 (4), 908–931.
Ardhuin, F., Rogers, E., Babanin, A.V., Filipot, J.F., Magne, R., Roland, A., van der Westhuysen, A., Queffeulou, P., Lefevre, J.M., Aouf, L., Collard, F., 2010. Semi-empirical dissipation source functions for ocean waves. Part I: Definition, calibration, and validation. Part II: Dissipation term and evolution tests. J. Phys. Oceanogr 40 (9), 1917–1941.
Badulin, S.I., Pushkarev, A.N., Resio, D.T., Zakharov, V.E., 2005. Self-similarity of wind-driven seas. Nonlinear Proc. Geophys. 12, 891–945.
Badulin, S.I., Babanin, A.V., Zakharov, V.E., Resio, D., 2007. Weakly turbulent laws of wind-wave growth. J. Fluid Mech. 591, 339–378.
Banner, M.L., Morison, R.P., 2010. Refined source terms in wind wave models with explicit wave breaking prediction. Part I: Model framework and validation against field data. Ocean Modell. 33 (1–2), 177–189 http://dx.doi.org/10.1016/j.ocemod.2010.01.002 .
Banner, M.L., Young, I.R., 1994. Modeling spectral dissipation in the evolution of wind waves. Part I: Assessment of existing model performance. J. Phys. Oceanogr. 24, 1550–1571.
Barnett, T.P., 1968. On the generation dissipation, and prediction of wind waves. J. Geophys. Res. 73, 529–531.
Benoit, M., 1992. Practical comparative performance survey of methods used for estimating directional wave spectra from heave-pitch-roll data. In: *Proceedings of 23rd International Conference on Coastal Engineering* (ASCE). Venice (Italy), pp. 62–75.
Birch, K.G., Ewing, J.A., 1986. Observations of wind waves on a reservoir. Inst. Oceanogr. Sci. Rep. No. 234, 37 pp.
Brucker, K., O'Shea, T., Dommermuth, D., Adams, P., 2010. Three dimensional simulations of deep-water breaking waves. In: 28th Symposium on Naval Hydrodynamics. Pasadena, CA, p. 19. 12-17 September 2010.
Chao, Y.Y., Alves, J.H.G.M., Tolman, H.L., 2005. An operational system for predicting hurricane-generated wind waves in the North Atlantic Ocean. Weather Forecast. 20, 652–671.
Cote, L.J., Davis, J.O., Marks, W., McGough, R.J., Mehr, E., Pierson, W.J., Ropek, J.F., Stephenson, G., Vetter, R.C., 1960. The directional spectra of a wind generated sea as determined from data obtained by the Stereo Wave Observation Project. Meteor. Pap. 2 (6), 1600–1604 New York University, New York.
D'Asaro, E.A., 2014. Turbulence in the upper-ocean mixed layer. Annu. Rev. Mar. Sci. 6, 101–115.
D'Asaro, E.A., Thomson, J., Shcherbina, A.Y., Harcourt, R.R., Cronin, M.F., 2014. Quantifying upper ocean turbulence driven by surface waves. Geophys. Res. Lett. 41 (1), 102–107.
Dommermuth, D., Rhymes, L., Rottman, J., 2013. Direct simulations of breaking ocean waves with data assimilation. In: Proceedings Oceans 2013, pp. 1–10. Sept. 2013.
Dommermuth, D., Yue, D., 1987. A higher order spectral method for the study of nonlinear gravity waves. J. Fluid Mech. 184, 267–288.
Donelan, M.A., Hamilton, J., Hui, W.H., 1985. Directional spectra of wind-generated waves. *Phil. Trans. R. Soc. London, A* 315, 509–562.
Donelan, M.A., Curcic, S.S., Chen, S., Magnusson, A.K., 2012. Modeling waves and wind stress. J. Geophys. 117, C00J23. doi:10.1029/2011JC007787.
Dysthe, K., 1979. Note on the modification of the nonlinear Schrödinger equation for application to deep water waves. In: Proc. R. Soc. London, A, 369, pp. 104–105.
Ewans, K.C., 1998. Observations of the directional spectrum of fetch-limited waves. J. Phys. Oceanogr. 28, 495–512.
Ewans, K.C., Kibblewhite, A.C., 1990. Spectral features of the New Zealand deep-water ocean wave climate. N. Z. J. Mar. Freshwater Res. 26, 323–338.

Ewing, J.A., 1971. A numerical wave prediction method for the North Atlantic Ocean. Dtsch. Hydorgr. Z 24, 241–261.
Forristall, G.Z., 1981. Measurements of a saturation range in ocean wave spectra. J. Geophys. Res. 86, 8075–8084.
Glazman, R.E., 1994. Surface gravity waves at equilibrium with a steady wind. J. Geophys. Res. 99, 5249–5262.
Grare, L., Lenain, L., Melville, W., 2013. Wave-coherent airflow and critical layers over ocean waves. J. Phys. Oceanogr. 43, 2156–2172.
Hasselmann, D.E., Dunckel, M., Ewing, J.A., 1980. Directional wave spectra observed during JONSWAP 1973. J. Phys. Oceanogr. 10, 1264–1280.
Hasselmann, K., 1962. On the non-linear energy transfer in a gravity wave spectrum. Part 1: General theory. J. Fluid Mech. 12, 481–500.
Hasselmann, K., et al., 1973. Measurements of wind-wave growth and swell decay during JONSWAP. Ergänzungsheft Dtsch. Hydrogr. Z. 12, 95.
Hasselmann, K., 1974. On the spectral dissipation of ocean waves due to white capping. Boundary-Layer Meteorol. 6 (1-2), 107–127.
Hasselmann, K., Muller, P., Sell, W., 1976. A parametric wave prediction model. J. Phys. Oceanogr. 6, 200–228.
Hasselmann, S., Hasselmann, K., Allender, J.Z.H., Barnett, T.P., 1985. Computations and parameterizations of the nonlinear energy transfer for application in wave models. J. Phys. Oceanogr. 15, 1378–1391.
Hasselmann, S., Hasselmann, K., 1985. Computations and parameterizations of the nonlinear energy transfer in a gravity-wave spectrum. Part I: A new method for efficient computations of the exact nonlinear transfer integral. J. Phys. Oceanogr. 15, 1369–1377.
Holthuijsen, L.H., 1983. Observation of the directional distribution of ocean wave energy in fetch-limited conditions. J. Phys. Oceanogr. 13, 191–203.
Hu, Y., Guo, X., Lu, X., Liu, Y., Dalrymple, R.A., Shen, L., 2012. Idealized numerical simulation of breaking water wave propagating over a viscous mud layer. Phys. Fluids 24, 112104.
Hwang, P., Wang, D., Walsh, E., Krabill, W., Swift, R., 2000. Airborne measurements of the wavenumber spectra of ocean surface waves. Part I: Spectral slope and dimensional spectral coefficient. J. Phys. Oceanogr. 30, 2768–2787.
Hwang, P., Wang, D., Walsh, E., Krabill, W., Swift, R., 2000. Airborne measurements of the wavenumber spectra of ocean surface waves. Part I: Directional distribution. J. Phys. Oceanogr. 30, 2753–2767.
Irisov, V., Voronovich, A., 2010. Numerical simulation of wave breaking. J. Phys. Oceanogr. 41, 346–364.
Jenkins, A.D., Phillips, O.M., 2001. A Simple formula for nonlinear wave–wave interaction. Int. J. Offshore Polar Eng. 11 (2), 81–96.
Kitaigorodskii, S.A., 1983. On the theory of the equilibrium range in the spectrum of wind-generated gravity waves. J. Phys. Oceanogr. 13, 816–827.
Komen, G.J., Hasselmann, S., Hasselmann, K., 1984. On the existence of a fully developed wind-sea spectrum. J. Phys. Oceanogr. 14, 1271–1285.
Korotkevich, A.O., Pushkarev, A., Resio, D., Zakharov, V., 2007. In: Kundu, A. (Ed.), Numerical Verification of the Hasselmann Equation, in the book "Tsunami and Nonlinear Waves". Springer ISBN: 978-3-540-71255-8.
Krogstad, H.E., 1990. Reliability and resolution of directional wave spectra from heave, pitch, and roll data buoys. Directional Ocean Wave Spectra. Johns Hopkins University Press, pp. 66–71.
Lin, R.Q., Perrie, W., 1999. Wave–wave interactions infinite depth water. J. Geophys. Res 104 (C5) 11, 193–1213.
Lin, M.Y., Moeng, C.H., Tsai, W.T., Sullivan, P.P., Belcher, S.E., 2008. Direct numerical simulation of wind-wave generation processes. J. Fluid Mech. 616, 1–30.
Liu, Y., 2013. Numerical study of strong free surface flow and breaking waves. Department of Civil Engineering, Johns Hopkins University PhD thesis.
Long, C.E, Resio, D., 2007. Wind wave spectral observations in Currituck Sound, North Carolina. J. Geophys. Res. 112, CO5001.
Longuet-Higgins, M.S., 1988, Mechanisms of Wave Breaking in Deep Water. Sea Surface Sound. In: Kerman, B.R. (Ed.). Springer, pp. 1–30.
Longuet-Higgins, M.S., Cokelet, E.D., 1976. The deformation of steep surface waves on water. I: A numerical method for computation. Proc. R. Soc. London 350A, 1–28.
Longuet-Higgins, M.S., Cokelet, 1978. The deformation of steep surface waves on water. II: Growth of normal mode instabilities. Proc. R. Soc. London 364A, 1–28.
Masuda, A., 1980. Nonlinear energy transfer between wind waves. J. Phys. Oceanogr 10, 2082–2093.
Miles, J.W., 1957. On the generation of surface waves by shear flows. J. Fluid Mech. 3, 185–204.
Miles, J.W., 1959. On the generation of surface waves by shear flows, Part 2. J. Fluid Mech. 6, 568–582.
Mitsuyasu, H., 1968. On the growth of the spectrum of wind-generated waves. Rep. Res. Inst. Appl. Mech., Kyushu Univ., 16, pp. 251–264.
Mitsuyasu, H., Tasai, F., Suhara, T., Mizuno, S., Ohkusu, M., Honda, T., Rikiishi, K., 1975. Observations of the directional spectrum of ocean waves using a cloverleaf buoy. J. Phys. Oceanogr. 5, 750–760.
Montoya, R.D., Osoria Arias, A., Ortiz Royero, J.C., Ocampo-Torres, F.J., 2013. A wave parameters and directional spectrum analysis for extreme waves. Ocean Eng. 67, 100–118.
Nwogu, O., 2009. Interaction of finite-amplitude waves with vertically sheared current fields. J. Fluid Mech. 627, 179–213.
O'Shea, T., Brucker, K., Dommermuth, D., Wyatt, D., 2008. A numerical formulation for simulating free-surface hydrodynamics. In: Proceedings of the 27th Symposium on Navak Hydrodynamics. Seoul, Korea.
Phillips, O.M., 1958. The equilibrium range in the spectrum of wind-generated waves. J. Fluid Mech. 4, 426–434.
Phillips, O.M., 1960. On the dynamics of unsteady gravity waves of finite amplitude. Part 1. J. Fluid Mech. (11) 143–155.
Pierson, W.J., Moskowitz, L., 1964. A proposed spectral form for fully developed wind seas based on the similarity theory of S.S. Kitaigorodskii. *J. Geophys. Res.* 69, 5181–5190.
Pushkarev, A., Resio, D., Zakharov, V., 2003. Weak turbulence approach to the wind-generated gravity sea waves. Phys. D 184, 29–63.
Pushkarev, A., Resio, D., Zakharov, V., 2004. Second generation diffusion model of interacting gravity waves on the surface of a deep fluid. Nonlinear Processes Geophys. 11, 329–342.
Resio, D.T., 1981. The estimation of wind-wave generation in a discrete spectral model. J. Phys. Oceanogr. 11 (4), 510–525.
Resio, D.T., Perrie, W., 1989. Implications of an f^{-4} equilibrium range for wind-generated waves. J. Phys. Oceanogr. 19 (2), 193–204.
Resio, D.T., Perrie, W., 1991. A numerical study of nonlinear energy fluxes due to wave–wave interactions in a wave spectrum. Part I: Methodology and basic results. J. Fluid Mech. 223, 603–629.
Resio, D.T., Long, C.E., Vincent, C.L., 2004. Equilibrium-range constant in wind-generated wave spectra. *J. Geophys. Res.* (Oceans) 109, C01018.
Resio, D.T., Perrie, W., 2008. A two-scale approximation for nonlinear energy fluxes in a wind wave spectrum Part I. J. Phys. Oceanogr. 38 (11), 2801–2816.
Resio, D.T., Long, C.E., Perrie, W., 2011. The role of nonlinear momentum fluxes in the evolution of the directional wind-wave spectrum. J. Phys. Oceanogr. 41, 781–801.
Romero, L., 2008. Airborne observations and numerical modeling of fetch-limited waves in the Gulf of Tehuantepec. E-scholarship at University of California, San Diego. https://escholarship.org/uc/item/8qq0b8br
Romero, L., Melville, W.K., 2010. Numerical modeling of fetch-limited waves in the Gulf of Tehuantepec. *J. Phys. Oceanogr*. 40, 466–486.
Siadatmousvi, S.M., Jose, F., Stone, G.W., 2012. On the importance of high frequency tail in third generation wave models. Coastal Eng 60, 248–260.
Sullivan, P., McWilliams, J.C., Moeng, C., 2000. Simulation of turbulent flow over idealized water waves. J. Fluid Mech. 404, 47–85.
Sullivan, P., McWilliams, J.C., Melville, W.K., 2004. The oceanic boundary layer driven by wave breaking with stochastic variability. I: Direct numerical simulations. J. Fluid Mech. 507, 143–174.
Sullivan, P.P, McWilliams, J.C., Patton, E.G., 2014. Large-eddy simulation of marine atmosphere above a spectrum of moving waves. J. Atmos. Sci. 71, 4001–4027.
Tanaka, M., 2001a. Verification of Hasselmann's energy transfer among surface gravity waves by direct numerical simulation of primitive equations. J. Fluid Mech. 444, 199–221.
Tanaka, M., 2001b. A method of studying nonlinear random field of surface gravity waves by direct numerical simulations. Fluid Dyn. Res. 28, 41–60.
Tanaka, M., 2007. On the role of resonant interactions in the short-term evolution of deep-water ocean spectra. J. Phys. Oceanogr. 37, 1022–1036.
Toba, Y., 1972. Local balance in the air–sea boundary processes. I: On the growth process of wind waves. J. Oceanogr. Soc. Jpn. 28, 109–121.
Toba, Y., 1973. Local balance in the air–sea boundary processes. III: On the spectrum of wind waves. J. Oceanogr. Soc. Jpn. 29, 209–220.
Toffoli, A., Onorato, M., Bitner-Gregersen, E.M., Monbaliu, J., 2010. Development of a bimodal structure in ocean wave spectra. J. Geophys. Res. 115.
Tolman, H.L, 2004. Inverse modeling of discrete interaction approximations for nonlinear interactions in wind waves. Ocean Modell. 6, 405–422.
Tolman, H.L., Grumbine, R.W., 2013. Holistic genetic optimization of a generalized multiple discrete interaction approximation for wind waves 2013. Ocean Modell 70, 25–37. doi:10.1016/j.ocemod.2012.12.008.
Tolman, H., 2013. A generalized multiple discrete interaction approximation for resonant four-wave interactions in wind wave models. Ocean Modell. 70, 11–24.
Tracy, B.A., and D.T. Resio, 1982: Theory and calculations of the nonlinear energy transfer between sea waves in deep water. WES Rep. No. 11. U.S. Army Engineer Waterways Experiment Stations, Vicksburg, MS.
Trulsen, K., Dysthe, K.B., 1996. A modified nonlinear Schrodinger equations for broader bandwidth gravity waves on deep water. Wave Motion 24, 281–289.
Tsagareli, K.N., Babanin, A.V., Walker, D.J., Young, I.R., 2010. Numerical investigation of spectral evolution of wind wave – Part I: Wind-input function. J. Phys. Oceanogr. 40, 656–666.
Van der Westheysen, A.J., Zijlema, M, Battjes, J.A., 2007. Nonlinear saturation-based white capping dissipation in swan for deep and shallow water. Coastal Eng. 54 (2), 151–170.
Wang, D.W., Hwang, P.A., 2001. Evolution of the bimodal directional distribution of ocean waves. J. Phys. Oceanogr. 31, 1200–1221.
Walsh, E.J., Hancock, D.W., Hines, D.E., 1988. An observation of the directional wave spectrum from shoreline to fully developed. J. Phys. Oceanogr. 19, 670–690.
WAMDI Group (13 authors), 1988. The WAM model – a third generation oceans wave prediction model. J. Phys. Oceanogr. 18, 1775–1810.
Webb, D.J., 1978. Nonlinear transfer between sea waves. Deep Sea Res 25, 279–298.
Xaio, W., Liu, Y., Wu, G., Yue, D., 2013. Rogue wave occurrence and dynamics by direct simulations of nonlinear wave-field evolution. J. Fluid Mech. 720, 357–392.
Yang, D., Shen, L., 2010. Direct-simulation-based study of turbulent flow over various waving boundaries. J. Fluid Mech. 650, 131–180.
Yang, D., Shen, L., 2011. Simulation of viscous flows with undulatory boundaries. Part II: Coupling with other solvers for two-fluid computations. J. Comput. Phys. 230, 5510–5531.
Yang, D., Meneveau, C., Shen, L., 2013. Dynamic modelling of sea-surface roughness for large-eddy simulation of wind over ocean wave field. J. Fluid Mech. 726, 62–99.
Young, I.R., Van Vledder, G., 1993. A review of the central role of nonlinear interactions in wind-wave evolution. Philos. Trans. R. Soc. London A342, 505–524.

Young, I.R., Verhagen, L.A., Banner, M.L., 1995. A note on the bimodal directional spreading of fetch-limited wind waves. J. Geophys. Res. 100, 773–778.
Zakharov, V.E., Filonenko, N.N., 1966. The energy spectrum for stochastic oscillation of a fluid's surface. Dokl. Akad. Nauk. 170, 1992–1995.
Zakharov, V.E., Zaslavskii, M.M., 1982. The kinetic equation and Kolmogorov spectra in weak-turbulence theory of wind waves. Izv. Atmos. Ocean. Phys. 18, 747–753.
Zhang, B., Perrie, W., 2012. Cross-polarized synthetic aperture radar: a new potential measurement technique for hurricanes. *Bull. Am. Meteorol. Soc.* 93 (4), 531–541.
Zhang, B., Perrie, W., Vachon, P., Li, X., Pichel, W., Guo, J., He, Y., 2012. Ocean vector winds retrieval from C-band fully polarimetric SAR measurements. IEEE Trans. Geosci. Remote Sens. 50, 4252–4261.